

RESEARCH ARTICLE

10.1029/2019JF005253

Key Points:

- The effective slope is one order of magnitude lower than the topographical slope in a step-pool stream
- The use of effective slope allows better predictions of bed load rates using empirical bed load formulas
- Tracer experiments in a step-pool stream reveal that the average flight displacement of sediments decreases for coarser sediment fractions

Correspondence to:

L. Mao,
lumao@lincoln.ac.uk

Citation:

Mao, L., Toro, M., Carrillo, R., Brardinoni, F., & Fraccarollo, L. (2020). Controls over particle motion and resting times of coarse bed load transport in a glacier-fed mountain stream. *Journal of Geophysical Research: Earth Surface*, 125, e2019JF005253. <https://doi.org/10.1029/2019JF005253>

Received 11 JUL 2019

Accepted 9 MAR 2020

Accepted article online 12 MAR 2020

Controls Over Particle Motion and Resting Times of Coarse Bed Load Transport in a Glacier-Fed Mountain Stream

Luca Mao^{1,2} , Matteo Toro³ , Ricardo Carrillo⁴ , Francesco Brardinoni⁵ , and Luigi Fraccarollo³ 

¹School of Geography, University of Lincoln, Lincoln, UK, ²Institute of Geography, Pontificia Universidad Católica de Chile, O'Higgins, Santiago, Chile, ³Department of Civil, Environmental and Mechanical Engineering, University of Trento, Trento, Italy, ⁴Department of Ecosystems and Environments, Pontificia Universidad Católica de Chile, O'Higgins, Santiago, Chile, ⁵Department of Biological, Geological and Environmental Sciences, University of Bologna, Bologna, Italy

Abstract Coarse bed load transport is a crucial process in river morphodynamics but is difficult to monitor in mountain streams. Here we present a new sediment transport data set obtained from 2 years of field-based monitoring (2014–2015) at the Estero Morales, a high-gradient stream in the central Chilean Andes. This stream features step-pool bed geometry and a glacier-fed hydrologic regime characterized by abrupt daily fluctuations in discharge. Bed load was monitored directly using Bunte samplers and by surveying the mobility of passive integrated transponder (PIT) tags. We used the competence method to quantify the effective slope, which is the fraction of the topographical slope responsible for bed load transport. This accounts for only 10% of the topographical slope, confirming that most of the energy is dissipated on macroroughness elements. We used the displacement lengths of PIT tags to analyze displacement lengths and virtual velocity of a wide range of tracer sizes (38–415 mm). Bed load transport in the Estero Morales shown to be size-selective, and the distance between steps influences the displacement lengths of PIT tags. Displacement lengths were also used to derive the statistics of flight distances and resting times. Our results show that the average length of flight scales inversely to grain size. This contradicts Einstein's conjecture about the linear relationship between grain size and intervals between resting periods in a steep step-pool stream in ordinary flood conditions.

1. Introduction

Sediment transport, flow resistance, morphological structure, and bed texture in rivers are interrelated in complex ways (Church, 2006). Coarse bed load transport in mountain streams is important for civil engineers, geomorphologists, river ecologists, and managers, as it determines channel morphology and dynamics, while representing a significant component of flood-related costs (e.g., Badoux et al., 2014). However, monitoring bed load in the field can be logistically onerous, costly, and affected by a number of uncertainties (Dell'Agnese et al., 2014; Magirl et al., 2015; Schneider et al., 2016; Vericat et al., 2006).

Predicting bed load is a difficult task, especially in steep mountain streams, where channel beds are often organized in boulder-cascade and step-pool morphologies (Brardinoni & Hassan, 2007; Buffington & Montgomery, 1997; Comiti & Mao, 2012). Modeling the flow over such bed structures is still very challenging (Escarriaza et al., 2017; Saletti et al., 2016), especially when levels of submergence are low (Comiti et al., 2009; Wilcox et al., 2011). Modeling flow and bed load transport in mountain stream is complex because patches of mobile sediments coexist with immobile structures such as steps or isolated boulders (Green et al., 2015; Laronne et al., 2001; Yager et al., 2012). Furthermore, critical dimensionless shear stress in mountain streams (i.e., Shields stress) is very difficult to model, due to its high variability in time (Masteller et al., 2019) and space (Monsalve et al., 2016), modulated by changes in local channel slope (Lamb et al., 2008) and relative submergence of sediments (Lenzi et al., 2006).

Only part of the flow power in mountain streams is available to entrain and transport sediments (Hohermuth & Weitbrecht, 2018; Rickenmann & Recking, 2011), as some energy is dissipated in various ways, including local hydraulic plunging and jumps over steps (Comiti et al., 2009; Green et al., 2013; Monsalve et al., 2017). In such complex hydraulic conditions, well-known and established flow resistance

approaches and empirical bed load formulas are unlikely to be reliable (e.g., Yager et al., 2018). Considering that mountain streams are typically supply limited (Lenzi et al., 2004; Turowski et al., 2009), bed load formulas fail to predict actual transport rates by orders of magnitude in step-pool streams (Nitsche et al., 2011), since not all the energy available is effective in transporting sediments. Because macroroughness can represent up to 90% of the total flow resistance in step-pool streams (Church & Zimmermann, 2007), accounting for the portion of energy slope or flow resistance associated with macroroughness can substantially increase the predictive power of empirical bed load formulas (Chiari & Rickenmann, 2011). Using a large empirical database, Rickenmann and Recking (2011) adopted Ferguson's (2007) approach for partitioning flow resistance and splitting the friction factor into a base level value associated with small-scale grain size roughness, and total value, which includes macroroughness, such as step pools. A similar breakdown can be applied to the topographical bed slope (i_b), from which an effective slope value (i_e), representing that part of the slope that plays a role in coarse grain entrainment and movement, can be extracted from the remaining part of the slope ($i_f = i_b - i_e$) associated with the mechanical power dissipated by flow over immobile bedforms (Nitsche et al., 2011).

Controls on sediment transport processes and dynamics in mountain streams can be explored using tracers. Displacement lengths of tracers depend on particle size and shear stress acting on them (e.g., Church & Hassan, 1992), but also on dimensionless impulse (e.g., Phillips et al., 2013) and antecedent flow conditions (e.g., Mao et al., 2017). Displacement length depends also on channel morphology and especially on the spacing between bedforms (Vázquez-Tarrio et al., 2019). Displacement length is needed to calculate the virtual velocity of sediment that can be used to assess coarse bed material transport (e.g., Brenna et al., 2019). Velocity is called virtual because it is usually calculated considering the interval between two consecutive surveys of tracers. However, tracers would naturally move through sequences of jumps and rest periods (Einstein, 1950) that are observable in laboratory experiments (e.g., Fraccarollo & Hassan, 2019) but difficult to monitor in the field, with only a few exceptions (e.g., Habersack, 2001; Maniatis et al., 2017).

In this paper, we use a new data set of direct bed load surveys in a step-pool stream to calculate the portion of slope effective in transporting sediments. We then use this slope value to analyze sediment transport dynamics and apply the Einstein (1950) and virtual velocity (Haschenburger & Church, 1998) approaches to characterize bed load mobility. Both approaches are based on a Lagrangian perspective of sediment transport which considers the motion of individual particles and views moving grains as being almost independent of each other. While sliding, rolling, and saltating over the bed, sediments may also experience long resting periods on the surface or may be temporarily buried as a result of temporal and spatial changes in the bed surface profile (Singh et al., 2009; Wong et al., 2007). Both the Einstein and the virtual velocity formulations allow for predicting bed load transport rates and can be expressed as a function of Shields stress, such as the MPM empirical bed load formula (Meyer-Peter & Muller, 1948; Wong & Parker, 2006). Here we will use field data to infer the predictors of Einstein's statistical approach. The study was conducted at the Estero Morales, a small glacier-fed Andean step-pool stream in central Chile. Coarse sediment mobility and transport rates were monitored in 2014–2015 using Bunte traps and passive integrated transponders (PIT) tagged clasts. The specific aims of the paper are to (i) use the competence approach to assess energy dissipation in step-pool morphology by calculating the effective slope of the stream; (ii) use the effective slope to assess the increase in the predictive power of a widely applied formula in a system with nearly unlimited sediment supply; (iii) use the virtual velocity of PIT tracers to assess sediment mobility; and (iv) assess the resting times of PIT tags using both particles that moved during the survey period and those that did not.

2. Study Site and Monitoring Methods

2.1. Study Site

The study was conducted in a reach of the Estero Morales, a high-gradient stream in the central Chilean Andes (Figure 1). The basin extends for 27 km², with an elevation between 1,780 and 4,497 m.a.s.l. There are several relatively small glaciers above 2,700 m.a.s.l. (Mao & Carrillo, 2017). Mean annual rainfall, as measured in the lower part of the basin, is around 550 mm. The climate is Mediterranean, with precipitation occurring mainly as snowfall from April to September, with occasional convective summer storms and late summer rain-on-snow events. The catchment is covered by snow for approximately 5 months a year, so discharge mainly results from snowmelt in late spring (from late September to November) and glacier melt from

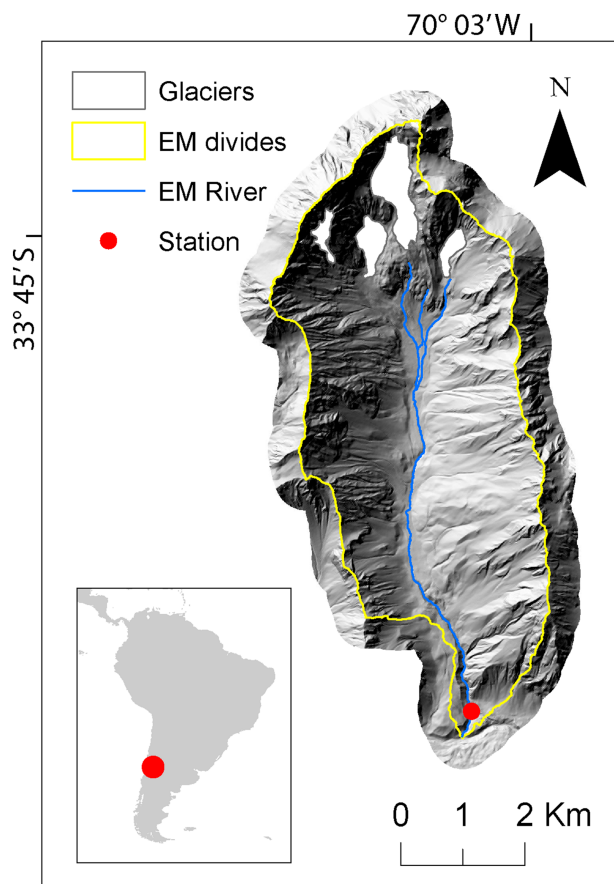


Figure 1. Location and map of the Estero Morales basin.

December to March. Bedrock geology of the catchment consists of volcanic metamorphic rock and conglomerate-sand deposits. The stream in the study reach is steep (0.14 m/m), and the channel width is approximately 7 m. The study reach is 760 m long and is located just upstream from the confluence with the El Volcan River (Figure 1). The stream flows through coarse lag deposits and features typical of step-pool sequences (Figure 2). In 2015, we counted 72 step-pool units over the 760-m-long reach, with an average spacing of approximately 10.5 m. The step-pool sequences are stable during ordinary glacial melting floods and are only prone to dislodgement and rearrangement during extreme late summer events. The site was monitored continuously from July 2013 until April 2016, when a high-magnitude event caused considerable channel changes and destroyed the monitoring devices.

2.2. Bed Load Monitoring and Sampling Using Bunte Traps

The study reach was equipped with a pressure transducer and a multi-parameter water quality probe (OTT Hydrolab MS5) to monitor water temperature, electrical conductivity, and turbidity with a 10-min time resolution (see Mao & Carrillo, 2017). A 0.5-m-long acoustic pipe sensor was also installed (Mao et al., 2016). A series of direct bed load samples were collected near the monitoring cross section using 0.3-m-wide and 0.25-m-high Bunte-type traps (Bunte et al., 2004). Two traps were located at points near the bed load acoustic pipe sensor (Figure 2), located on the sampling site (Figure 1). Samples were collected during the glacier melting season (January to March) in 2014 and 2015 at discharges ranging from 1 to 3 m³/s¹. The highest discharge monitored was roughly the bankfull discharge. The highest discharge in the Estero Morales (approximately 7 m³/s¹) was recorded in April 2016 and was able to destroy and recreate step pools (Mao & Carrillo, 2017). Sampling was concentrated in a few days to monitor bed load at a wide range of transport rates.

Multiple samples were taken, especially during the rising limb of hydrographs. The duration of bed load sampling ranged from 1 to 120 min depending on the discharge. The amount of trapped sediment ranged from 0.1 to 49.7 kg. The sediment collected in the traps was dried, weighed, and later sieved in the laboratory.

2.3. Bed Load Monitoring Using Tracers

Coarse sediment mobility in Estero Morales was also investigated using natural clasts equipped with 23-mm-long radio frequency identification (RFID) passive integrated transponder tags (Hassan et al., 2013; Liébault et al., 2012). PIT tags are transmitters without batteries that emit an identification codes by radio frequencies, which are detected and recorded. The RFID PIT system uses electromagnetic fields to automatically identify tags. A commercially available mobile RFID system consisting of a reader unit, a battery supplying the system, a screen, and a short-range antenna (0.5 m in diameter) was used to determine the position of PIT tags (Figure 2). The antenna can generally recognize tracers in a range of 0.3 m, although this varies depending on the position of the clast relative to the antenna, the battery charge, and interference among PIT tags (see Chapuis et al., 2014).

PIT tags were inserted in holes drilled in the clasts and closed using epoxy glue. The three main dimensions of the clasts (a, long; b, medium; and c, short) were measured with a caliper, and the clasts were weighed to determine the relationship between b-axis diameter and weight. Only sediments collected in the Estero Morales were used to produce PIT tracers for this study. The tracers were also spray-painted to enhance their visibility in the channel bed. The PIT tags were placed in the upstream end of the study reach and ended up at the confluence with the El Volcan River. As in other studies (e.g., Dell'Agnese et al., 2015), the PIT tags were laid in the channel bed and gently pushed by foot into the surface sediment material to prevent them from protruding abnormally from the bed. PIT tags were always inserted at three transects (spaced 0.5 m apart) at the upstream end of the reach. The operator equipped with the mobile antenna scanned the channel bed surface for tags. When a tag was detected, vertical and horizontal distance were measured



Figure 2. Views of the Estero Morales (a) at the monitored cross section; (b) at the upstream end of the reach where the PIT tracers were placed and surveyed; (c) during a PIT survey conducted with a portable antenna; and (d) during bed load sampling using Bunte traps. The channel width is about 7 m.

from wooden stakes with a laser rangefinder. Overall, 32 wooden stakes were located along the study site, and all were georeferenced using DGPS. At the beginning of the measuring periods in January 2014 and January 2015, 461 and 395 PITs respectively were placed in the study reach during low-flow conditions. PIT positions were surveyed 20 times in 2014 and 13 times in 2015. Each survey took 1 to 2 days and required intense in-channel surveys, carried out by two operators, who worked until 2 p.m., after which increased discharge made the search for PITs unsafe. The flow regime during the monitoring search for PITs was always characterized by daily fluctuations in discharge. The surveys always started from the upstream end of the monitored reach. Due to the rapid increase in water discharge in the early afternoon, it was generally possible to survey only the upper half of the reach. On one occasion, it was possible to survey the entire reach. Figure 3 shows the size distribution of the tracers, and the bed surface and subsurface sediments. A surface grid-by-number sampling revealed that the sediments are coarse and

poorly sorted ($D_{16} = 20$; $D_{50} = 59$; $D_{84} = 318$; and $D_{90} = 448$ mm; Figure 3). A volume-by-weight subsurface sampling showed that bed material grain size distribution is finer than that of the surface, demonstrating a certain rate of surface armoring ($D_{50-sub} = 25$ mm; Figure 3). The b-axes of tracers range from 27 to 420 mm. The lower value of this range was determined by the length of the PIT tags inserted in the clasts (23 mm), and the upper value by the size of pebbles in which PITs could be inserted and then transported in the study site.

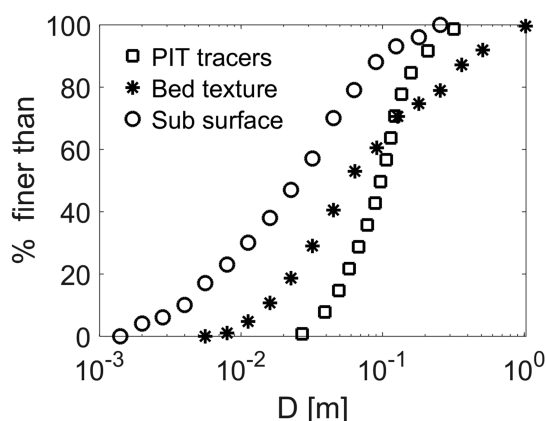


Figure 3. Surface and subsurface grain size distribution in the monitored reach of the Estero Morales, and size distribution of PIT tracers.

3. Conceptual and Theoretical Framework: Unifying the Statistical Motion and Virtual Velocity Approaches

In this section, we introduce Einstein's (1950) bed load formula and present the way field data collected with the PIT tracers was used to back-calculate the predictors that appear in the formula. Einstein's pioneering approach describes the bed load transport rate as a function of two predictors that consider the probabilistic distribution of mean

particle displacements \bar{L} and \bar{T}^{-1} , being T the resting time. L represents the distance that a particle runs without pausing during its movement from an entrainment to the subsequent deposition. We refer to this as flight distance, whereas in other studies (e.g., Bradley et al., 2010; Habersack, 2001; Nikora et al., 2002) it is termed step or travel distance, quick length step, intermediate trajectories, and travel distance. T is the resting time, that is, the time interval from a first deposition to the next entrainment, whereas T^{-1} represents the probability for a single grain at rest to be entrained in a unit of time. The Einstein expression has two further factors, which are constant for a given bed, that is, the number N of grains paving a unit area and the reference volume \forall of a single particle. N can be evaluated as the ratio between bed particle concentration c_b (volumetric percentage of solid volumes) and the particle reference cross section A . Following the above notations, the Einstein (1950) formulation for the unit volumetric transport rate q_s (in m^2/s) is expressed as

$$q_s = \bar{T}^{-1} \forall \frac{c_b}{A} \bar{L}. \quad (1)$$

In order to make equation 1 applicable to all i th grain size classes of a poorly sorted mixture, we add a factor f_i , which indicates the volumetric frequency of the class size D_i , resulting in

$$q_{si} = \bar{T}_i^{-1} \forall_i \frac{c_b}{A_i} \bar{L}_i f_i, \quad (2)$$

where \forall_i is the reference volume of a single particle in the i^{th} grain size class. The term $\bar{T}_i^{-1} \frac{c_b}{A_i}$ can be termed E_i , which represents the number of particles entrained per unit of time and unit of bed surface area. Unless the probability distribution of the resting times is uniform, it holds that

$$\bar{T}_i^{-1} \neq \frac{1}{\bar{T}_i}. \quad (3)$$

The ratio \forall_i/A_i is equal to αD_i , α being a constant. Indeed, for nearly spherical-shaped grains it holds that $\forall_i/A_i = \frac{4}{3} \pi \frac{D_i^3}{8} / \pi \frac{D_i^2}{4} = \frac{2D_i}{3}$. Thus, it is generally true that α is close to unity and depends on the shape of the particle. Eventually, equation 2 becomes

$$q_{si} = \alpha D_i c_b \bar{T}_i^{-1} f_i \bar{L}_i. \quad (4)$$

The distribution of \bar{T}_i can be obtained from the data set collected in the field using the tracers (see section 6).

The unit volumetric transport rate q_s (per unit of width of the active channel) in the virtual velocity approach can be calculated for well-sorted sediments as follows (Haschenburger & Church, 1998; Hassan & Bradley, 2017; Liébault & Laronne, 2008):

$$q_s = V_v \delta c_b, \quad (5)$$

where c_b is the volumetric concentration of the sediments in the bed and δ is the thickness of the active layer of sediments. The virtual velocity of bed load V_v is calculated as the ratio between the displacement ℓ traveled by a particle in a certain time interval t , and t itself. Because particles are entrained, moved, and rested several times during a transport event, it holds that t is much longer than the above defined T and that the displacement ℓ is much longer than the previously defined \bar{L} . Virtual velocity V_v is thus the averaged velocity, over both motion and resting periods, of a large ensemble of grains running their trajectory. The transport of each i th grain size fraction of a poorly sorted bed mixture, given its volumetric fraction f_i in the bed mixture, and its representative grain size D_i , is given by

$$q_{si} = V_{vi} \delta c_b f_i. \quad (6)$$

In this paper, we use the data collected with PIT tracers in sequential surveys to calculate the virtual sediment velocity V_v , considering the time elapsed from when a trace was inserted in the bed (or the previous

survey) until the last time it was detected, and the distance traveled from the release (or the previous survey) to the position at which it was last recovered (as is usually done in literature, see Vázquez-Tarrio et al., 2019). From equation 6 it can be drawn that

$$V_{vi} = q_{si}/c_b \delta f_i. \quad (7)$$

With the aim of establishing a relation between the two approaches, equations 2 and 7 can be combined as

$$q_{si} = \alpha D_i c_b \overline{T_i^{-1}} f_i \overline{L_i} = V_{vi} \delta c_b f_i. \quad (8)$$

Equation 8 yields

$$V_{vi} \approx \overline{T_i^{-1}} \overline{L_i} \frac{\alpha D_i}{\delta}, \quad (9)$$

which displays a straightforward interpretation of virtual velocity in terms of predictors in Einstein's approach. Interestingly, equation 9 applies to both well and poorly sorted bed mixtures.

4. Effective Slope and Predictive Power of Empirical Bed Load Formulas

Around two thirds of the total energy in steep streams can be dissipated in the hydraulics generated by step-pool sequences (e.g., Wilcox et al., 2011), and this dissipated energy does not contribute to generating bed load transport. Here we apply a slope decomposition approach (as in Nitsche et al., 2011), in which the mean topographic longitudinal slope i_b is split into the effective slope involved in sediment transport (i_e) and the component of slope that is absorbed in form and spill drags (i_f):

$$i_b = i_e + i_f. \quad (10)$$

To calculate the effective slope i_e , we used the competence approach for incipient sediment motion, which considers the largest particle transported and collected during bed load samplings conducted under different hydrometric conditions (Andrews, 1983; Batalla & Martín-Vide, 2001; Mao et al., 2008). In the case of the Estero Morales, we used the size of the coarsest grain captured with the Bunte traps (D_{100}) and the shear stress acting on the bed calculated using the depth-slope approach (Wilcock, 1993), which involves the use of the water depth at the time of sampling (h), topographical slope (i_b), the acceleration constant due to gravity (g), and water density (ρ). The shear stress associated with sediment transport is calculated as

$$\tau = h i_b g \rho. \quad (11)$$

Here we adopted the flow competence method, which assumes that the local flow conditions at the moment of bed load sampling can be considered critical for the entrainment and transport of the coarsest sediment trapped in the sampler (Andrews, 1983; Lenzi et al., 2006). In other words, the shear stress during a bed load sampling is critical for the coarsest particles found in the Bunte trap (D_{100}), and thus the critical Shields stress (θ_{cr}) can be calculated as

$$\theta_{cr} = \frac{h \cdot i_b}{\Delta \cdot D_{100}}, \quad (12)$$

where $\Delta = \rho_s/\rho - 1$ and ρ_s is the density of sediments. If i_e , rather than i_b , is considered in equation 12, the effective slope can be calculated as

$$i_e = \frac{\theta_{cr} \cdot \Delta \cdot D_{100}}{h}, \quad (13)$$

which shows that the ratio D_{100}/h is proportional to i_e , provided that θ_{cr} is assumed to be constant. Figure 4 shows the relationship between transported D_{100} and the water depth at the time of direct bed load sampling conducted in 2014 and 2015. The size of the coarsest transported sediments increases with the flow depth, although the predictive power of a linear regression is very weak ($R^2 = 0.29$). The considerable scatter of

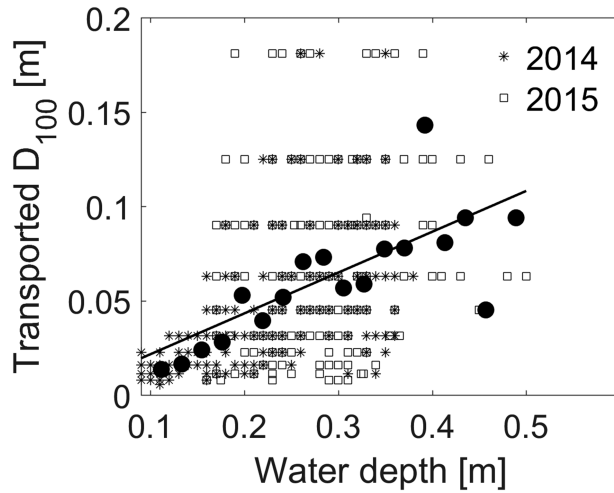


Figure 4. Relationship between the coarsest clast (D_{100}) collected with the Bunte sampler and the water depth at the time of sampling, as measured at the monitoring site during events recorded in 2014 and 2015. The filled black dots represent the average values of D_{100} for binned classes of water depth. The regression plots as $D_{100} = 0.2436 h - 0.0056$ ($R^2 = 0.29$).

data is consistent with previous observations (e.g., Mao et al., 2008). On the one hand, this could be attributed to the reduced trapping efficiency of Bunte samplers, especially at higher bed load transport rates due to shorter sampling times and the fact that D_{100} approaches the size of the sampler intake. On the other hand, the scatter observable in Figure 4 is also due to the natural grain size variability of upstream sediment delivery sources, dynamics of destruction of sediment clusters, changes in sediment imbrication, and temporal variability of local shear stress. As well, the flow conditions at the bed load sampling point are unlikely to represent the local conditions well in the place where the sediments were entrained, causing further scatter in the relationship between the coarsest clast captured by the sampling basket and the water stage at the site of monitoring.

The effective slope can be calculated by assuming a certain value of the critical Shields parameter θ_{cr} unaffected by grain sorting, particle size interactions, channel slope, or high relative roughness. Although the critical Shields parameter can vary locally, ranging from 0.03 to 0.09 (Buffington & Montgomery, 1997), if an intermediate value of 0.05 is assumed, equation 13 provides a calculated value of i_e of 0.018 m/m. Interestingly, this value of effective slope is almost one order of magnitude

lower than the actual mean topographic channel slope ($i_b = 0.14$ m/m), revealing that only a small part of the available bed shear stress is actually associated with sediment transport during ordinary daily floods in the Estero Morales. This is well in agreement with the high level of energy dissipation associated with bedforms (Chin & Wohl, 2005; Comiti et al., 2009), which can account for 80% of the total flow resistance (e.g., Canovaro et al., 2007; Chiari et al., 2010; Wilcox et al., 2011).

Our calculation of effective slope can be compared with the effective slope estimated using the power-function relation proposed by Rickenmann and Recking (2011):

$$\frac{i_e}{i_b} = (i_b^{-z} p)^e, \quad (14)$$

where $p = 0.07$, $z = 0.47$, and $e = 1.2$ were calibrated using a large empirical data set (Chiari & Rickenmann, 2011; Rickenmann & Recking, 2011). For the Estero Morales, equations 13 and 14 provide an estimate of i_e/i_b , of around 0.13, remarkably similar to the ratio resulting from the use of the value of i_e (0.018 m/m, see above), confirming that the analysis based on competence is sound. Notably, Nitsche et al. (2011) combined several bed load transport and flow resistance equations to account for flow energy dissipation of step-pool morphology in steep streams. They recommended using the slope decomposition approach (i.e., Rickenmann & Recking, 2011) to increase the predictive power of bed load formulas that generally overestimate bed load transport in mountain streams by orders of magnitude (e.g., Vázquez-Tarrio & Menéndez-Duarte, 2015). Here we use effective slope to assess the increase in the predictive power of a widely applied formula in a system with nearly unlimited sediment supply and to derive the reference values needed for the later development of the present work. Specifically, we applied the Meyer-Peter and Muller equation (Meyer-Peter & Muller, 1948; Wong & Parker, 2006, hereafter MPM) using both the effective slope i_e and the topographical slope i_b , to calculate the value of the Shields parameter θ_{50} as

$$\theta_{50(i_e)} = \frac{h \cdot i_e}{\Delta \cdot D_{50}}; \theta_{50(i_b)} = \frac{h \cdot i_b}{\Delta \cdot D_{50}}, \quad (15)$$

where h is the water depth measured in the field at the monitoring station and D_{50} is the median grain size. Figure 5 shows the typical daily fluctuation of θ_{50} over several days during the monitoring season, calculated with the effective slope i_e . The value of θ_{50} calculated with topographical slope would be one order of magnitude higher. The outcome using topographical slope would suggest that bed load even occurs at the lowest discharges at night. In contrast, effective slope provides values of shear stress ranging from 0.030 to 0.075.

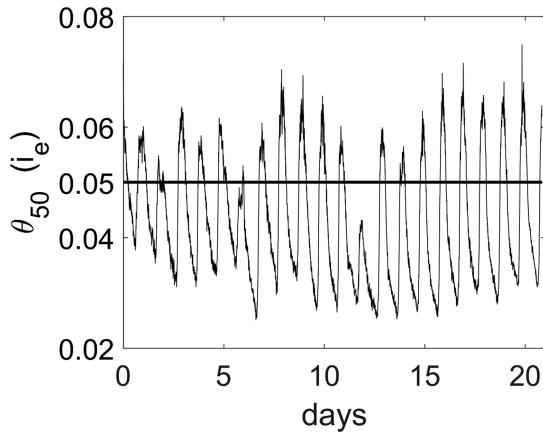


Figure 5. Temporal trend of the dimensionless shear stress over three exemplary weeks of January 2014 in the Estero Morales calculated with equation 15 using the effective slope i_e . The horizontal line refers to the assumed critical value of shear stress ($\theta_{50(i_e)} = 0.05$), which corresponds to a value of Shields of almost 0.40 if calculated using the topographical slope i_b .

expected, bed load rate increases with shear stress, rising from $5 \times 10^{-8} \text{ m}^2/\text{s}$ at Shields of 0.03 to $5 \times 10^{-5} \text{ m}^2/\text{s}$ at Shields of 0.06, and the values of volumetric bed load rates are rather scattered. Figure 7 shows instead the values of bed load rates versus the water stage at the time of sampling. This graph allows plotting the MPM predictions calculated using both i_e and i_b showing that using topographic slope to calculate MPM results in overestimating bed load transport rates by more than one order of magnitude (Figure 7). Conversely, MPM predictive power increases substantially when the effective slope is used, especially at the higher transport rates.

The use of effective slope is therefore a promising way to increase the predictive power of empirical bed load formulas developed in flume experiments, in order to account for energy dissipation due to morphological units, such as step pools, which are usually associated with high slope (Rickenmann & Recking, 2011). Indeed, the presence of step pools produces a large apparent increase in Shields stress (Chin & Wohl, 2005; Mao et al., 2008) and can strongly affect bed load prediction (Recking et al., 2016).

It is worth stressing here that the reach-averaged shear stress calculated with equation 11 is based on several assumptions (i.e., topographical slope is equal to the water slope and to the energy slope) that

are hardly met in steep streams like the Estero Morales (see Yager et al., 2018). In future attempts, better estimates of effective slope and predictions of bed load rates could be achieved by monitoring the slope of the water surface or local flow velocity or by using 2-D flow models to estimate the near-bed shear stress (e.g., Monsalve et al., 2016).

The analysis also provides further insights into the transport regime of Estero Morales during summer glacial melting floods. As previously suggested (Berzi & Fraccarollo, 2013; Capart & Fraccarollo, 2011), the Shields value can discriminate between ordinary (low Shields) and collisional (high Shields) bed load regimes for non-cohesive coarse sediments in turbulent flows. Shields stress in the Estero Morales calculated using effective slope is around 0.1, which suggests the occurrence of an ordinary bed load transport regime in which sediment moves by sliding and saltation, with prolonged rest periods, as was observed in the field. In contrast, the application of the topographical slope i_b suggests an intense collisional regime in which particles also frequently collide.

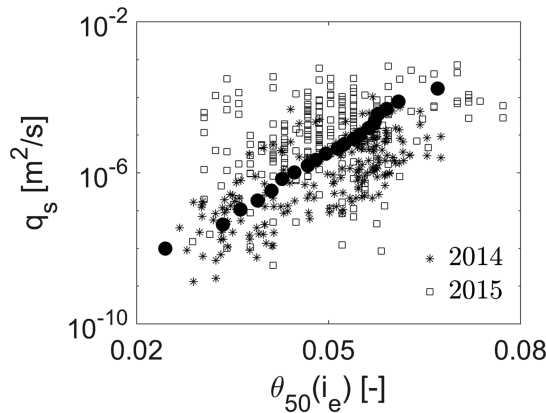


Figure 6. Bed load transport rates as measured with the Bunte traps in 2014 and 2015, plotted against the Shields parameter calculated using the effective slope. The filled black dots represent the average values of q_s for binned classes of shear stress.

The shear stress calculated with equation 15 can be then applied to the revised MPM equation (Wong & Parker, 2006) to evaluate sediment transport rates. If applied to well-sorted mixtures, the MPM reads as

$$q_s^{MPM} = 4(\theta - \theta_{cr})^{3/2} (g\Delta)^{1/2} D_{50}^{3/2}, \quad (16)$$

where q_s^{MPM} represents calculated solid discharge per unit of active channel width. For poorly sorted mixtures, the unit solid discharge can be calculated for each grain size fraction D_i as follows:

$$q_{si}^{MPM} = 4f_i(\theta - \xi_i\theta_{cr})^{3/2} (g\Delta)^{1/2} D_i^{3/2}, \quad (17)$$

f_i being the volumetric frequency of each i th grain size class and ξ_i the hiding factor calculated as $\xi_i = (D_i/D_{50})^{0.905}$, as previously suggested (Andrews, 1983; Parker et al., 1982). The instantaneous value of q_s^{MPM} is calculated using a value of the Shields stress obtained from equation 15, where the flow depth is provided by the local water stage meter.

Figure 6 shows bed load rates measured using Bunte samplers versus the dimensionless shear stress calculated using the effective slope i_e . As

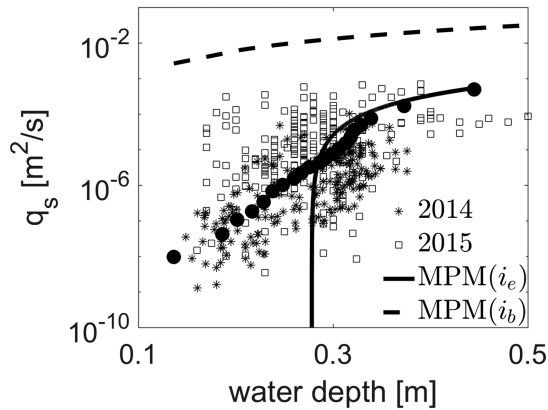


Figure 7. Bed load transport rates plotted against the water depth at the time of sampling. The filled black dots represent the average values of q_s for binned classes of water depths. The figure shows that the Meyer-Peter-Mueller equation predicts the order of magnitude of bed load rates if the Shields stress is calculated using i_e , but overestimates actual transport rates by more than two orders of magnitude if calculated using i_b .

($\theta_{50} > \theta_{cr}$). Following this logic, we calculated the average virtual velocity of each PIT tracer using their traveled distance and 30% of the time interval between the two subsequent surveys, irrespective of the survey date.

The virtual velocity of particles of different sizes can be used to quantify the volumetric bed load transport rates using equation 6, which also requires the thickness of the active layer δ . The thickness of the active sediment layer generally depends on local hydraulic conditions and bed texture (e.g., Houbrechts et al., 2012).

Although δ depends on the shear stress acting locally (Brenna et al., 2019; Kumbhakar et al., 2018; Wilson, 1987), it can be reasonably assumed that the thickness of the active layer is proportional to the surface grain size $\delta = a D_{50}$ (Haschenburger & Church, 1998) with a ranging from 1 to 3 (Hassan & Bradley, 2017). Einstein (1950) originally estimated a as twice the surface grain size. As a first approximation in this paper, we assume that the thickness of the active layer is equal to the median surface grain size. This is reasonable during the ordinary fluctuations of discharge monitored in 2014 and 2015, as only a few tracers were found buried during the surveys. Given that the step pool remained stable over the 2 years of observations, this indicates that only minor vertical adjustments occurred in the channel bed. Arguably, the assumption that $\delta = D_{50}$ would not hold true for higher-magnitude events that affect the stability of step-pool sequences, as the thickness of the active layer would become larger and affected by erosion/deposition dynamics.

The above considerations on how to evaluate the virtual velocity and the active layer in the field are useful in considering equation 7.

If bed load transport rates q_{sl} are calculated using the MPM formula based on the effective slope (equation 17; Figure 7), equations 7 and 17 are combined to obtain V_{vi} in m/day:

$$V_{vi} = \frac{1}{0.3 D_{50}} \int_{1 \text{ day}} q_{sl}^{MPM} dt. \quad (18)$$

Here we assume a value of c_b equal to 1, and a grain size distribution range corresponding to that of the PIT population, thus underrepresenting the finer fractions, to some extent. In equation 18 V_{vi} represents the virtual

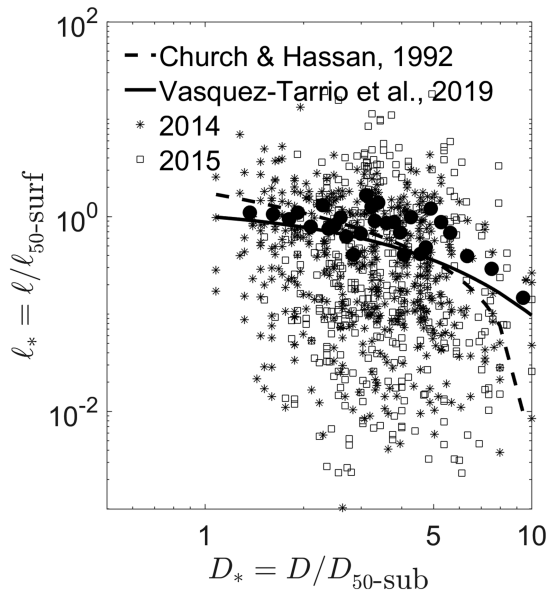


Figure 8. Dimensionless displacement ℓ^* of individual particles (scaled by the averaged travel distance of particles similar to the surface size D_{50}) as a function of dimensionless particle size D^* (scaled by the subsurface median size). The best fit regression is $\ell^* = -0.296 D^* + 2.389$ ($n = 517$; $p < 0.001$; $R^2 = 0.095$). The filled dots represent the average values of dimensionless displacements for binned classes of dimensionless particles sizes. Empirical equations of Church and Hassan (1992) and Vázquez-Tarrio et al. (2019) are plotted as well.

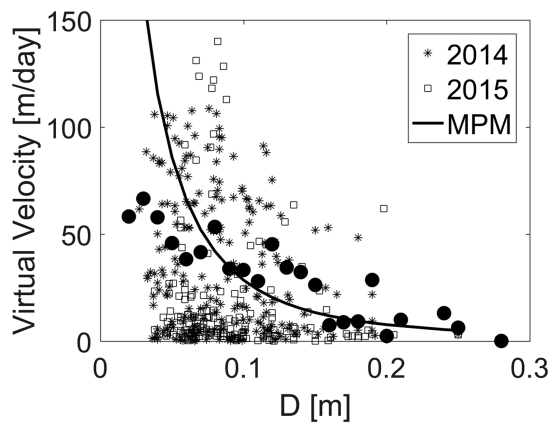


Figure 9. Virtual velocities plotted against the size of tracers used in the Estero Morales. The filled dots represent the average values of virtual velocity for binned classes of particles sizes. The solid line represents equation 18.

velocity (m/day) averaged over the portion of the day when $\theta_{50} > \theta_{cr}$. The two sides of equation 18 are plotted against grain size in Figure 9. As documented elsewhere (e.g., Liébault et al., 2012), despite the high degree of scatter, virtual velocities tend to decrease hyperbolically with grain size. This behavior is reproduced fairly well by the MPM volumes calculated when the hiding effect (see equation 17) and effective slope are considered. On the contrary, using topographical rather than effective slope in the calculation of bed load transport rates would result in a major overestimation of virtual velocity, especially of the coarser fractions, consistently with results in Figure 7. The overall reduction of virtual velocities with grain size indicates that the shear stress exerted by the flow over the bed during a daily flood is never high enough to make the size of transported sediment independent of critical Shields stress (e.g., the transport is size-selective) and confirms that the sediment transport regime belongs to the ordinary bed load mode.

The tracer data show virtual velocities of up to 65 m/day (looking at the binned data in Figure 9) and null values for grain size coarser than 250 mm. These values are representative of the flow conditions obtained

by restricting the analysis to intraday sub-periods characterized by $\theta > \theta_{cr}$ (see Figure 5). Clearly, if averaged over an entire day, including periods at $\theta < \theta_{cr}$, when no bed load transport occurs, we would obtain lower virtual velocity.

6. The Statistics of Sediment Resting Times and The Einstein Conjecture

Ordinary tracer studies focus on the mobility and virtual velocity of sediments during floods. Frequent subsequent surveys with the mobile antenna, combined with the natural daily fluctuations in discharge, allowed us to focus on the tracers that remained in the same location over two or more surveys in order to calculate sediment resting times. The field surveys conducted over consecutive days allowed for directly estimating the resting times T_i of the PIT tags of different grain sizes. When a tracer was recovered in the same position in the following survey, the resting time was calculated, representing the time interval elapsing from the first to last retrieval in the same position. Using these direct measurements, the mean resting time obtained by averaging all the PITs is approximately 8.6 days. If the resting times are calculated using the portion of the day when $\theta > \theta_{cr}$ (which represents approximately 30% of the time, see Figure 5), the mean resting time drops to around 2.6 days of continuous over threshold flow with active bed load transport. Figure 10 reports the values of these directly measured resting times (red dots) as a function of tracer size. The lack of data points for durations of less than 8 hr (30% of a day, when $\theta > \theta_{cr}$) is related to the temporal resolution of field surveys (i.e., at least 1 day apart from each other), which is an intrinsic limitation of

non-continuous tracking. Interestingly, the resting times are not sensitive ($R^2 = 0.03$) to the grain size of tracers, indicating that the probability of a grain in the Estero Morales being entrained is independent of its size (Figure 10).

Figure 10 also shows a series of resting times calculated indirectly, derived from a re-evaluation of the Einstein approach along with the empirical resting times derived from repeated field surveys. The method used to calculate this data set is explained below.

We took advantage of the fact that any measured PIT displacement is the cumulative distance traveled over a known inter-survey time interval, without taking into account that particles tend to move on subsequent jumps that include multiple stops with relative resting times. Conceptually, at least one resting time is associated with any single flight (i.e., a distance > 0) that took place during an inter-survey interval. We developed a method to work with these data and extract one or more resting time from any inter-survey displacement. In Einstein's (1950) bed load

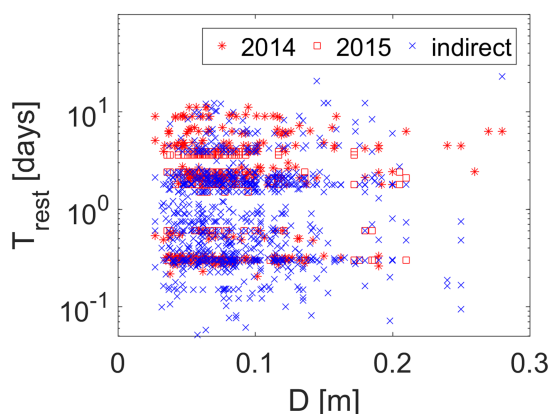


Figure 10. Resting times of coarse particles directly measured or computed through displacement surveys of PIT tags.

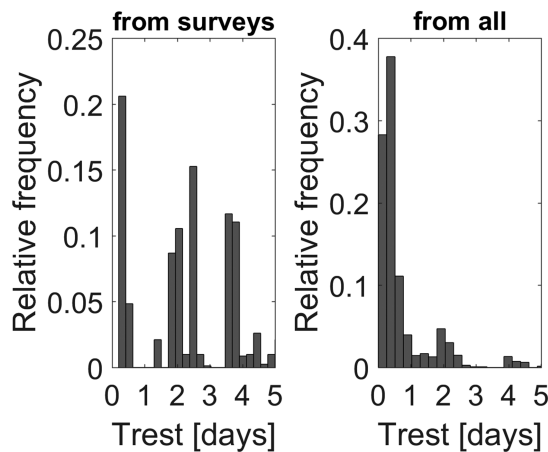


Figure 11. Histograms of the rest periods from direct surveys (left panel), and all rest periods including those calculated through displacement surveys (right panel).

formula (equation 2), the flight distance L_i is assumed to depend on the size of the sediment D_i and on ω , a positive dimensionless constant ($\omega \approx 100$):

$$\bar{L}_i = \omega D_i. \quad (19)$$

Given that L_i depends only on D_i (see equation 19), in Einstein formula the bed load intensity depends completely on the other predictor E_i representing the number of particles entrained per unit time and unit bed surface area. In order to interpret our data set, we relaxed the Einstein constraint and adopted the following linear relationship:

$$\bar{L}_i = \omega D_i + c. \quad (20)$$

The constant c makes it possible, at least theoretically, to obtain a negative value of the coefficient ω , which is always positive in experimental studies (Campagnol et al., 2012). The presence of c also implies that there are parts of the bed surface occupied by stable bed-form structures over which

particles do not stop during ordinary events (i.e., floods are not able to destroy bedforms). As in Einstein (1950), equation 20 assumes that the coefficients are constant and independent of both grain size and bed load intensity.

By applying a recursive procedure, we obtained L_i and a rich sample of resting times that together contribute to describing the distribution of the directly measured resting times. In the first iteration of the procedure, which started with guess values of ω and c (e.g., the Einstein's values, $\omega = 100$ and $c = 0$ m), we used equation 20 to calculate L_i for all grain sizes. Each measured inter-survey displacement was divided by L_i to obtain the number of resting periods the particle underwent during such displacement. The inter-survey time interval was thus divided by the number of resting periods to calculate the duration of each one. These additional and indirect values enrich the statistics of the resting times, summing to those directly measured in the field.

All the values of resting times, both directly measured and inferred from the displacements, were used to calculate a mean value \bar{T} . We then used the measured average values of virtual velocity for each grain size (see Figure 9) to indirectly obtain the average flight distance L_i based on the grain size. This is accomplished by multiplying the virtual velocity, which depends on the grain size (we used the binned values reported in Figure 9), by \bar{T} . Based on these values of L_i , the parameters ω and c were back-calculated, using equation 20, and iterations were repeated until the values of ω and c remained constant.

Figures 10 and 11 illustrate the results obtained at the end of the direct and indirect approaches of the calculation. Neither directly measured data (red dots in Figure 10) nor the indirect data extracted from displacements (blue dots in Figure 10) show significant dependence of resting times on grain size. Figure 11 shows the statistical distribution of resting times of the two data sets. The directly measured resting times display an unclear probability-density distribution (Figure 11), which becomes better constrained when measured and displacement-inferred resting times are merged (Figure 11b). Their overall mean is about 32 hr (1.35 days). The directly measured and the displacement-inferred resting times concur when below-threshold periods (i.e., when the Shields value is below the critical level) have been removed. Because θ exceeds θ_{cr} for approximately 30% of the time, an effective mean period \bar{T} of 32 hr represents on average 4.5 days in the monitored reach of Estero Morales. Figure 11 clearly indicates that the inequality reported in equation 3 fully applies, as the probability-density distribution of the resting times is far from being uniform.

Our results further show that the relation between L_i and D_i does not confirm Einstein's assumption that $\omega = 100$ and $c = 0$ m. Indeed, the flight distance of single grains decreases with particle size, and we obtained values of ω and c of $-200 [-]$ and 50 m, respectively (Figure 12). Interestingly, ω is negative, revealing that in a naturally structured step-pool channel experiment, sediment mobility is completely different from that in flume runs with well-sorted sediments and no bedforms (Campagnol et al., 2012; Fraccarollo & Hassan, 2019;

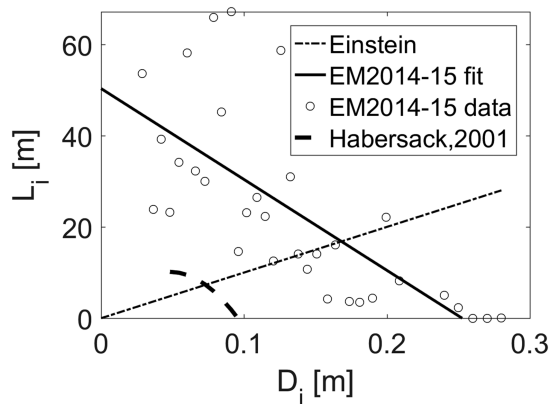


Figure 12. Experimental data of flight displacement versus grain size, including the best fit of equation 20. Einstein's line represents $L_i = 100D_i$. The empirical equation of Habersack (2001), applied using D_{50} of the Estero Morales, is plotted as well.

Lajeunesse et al., 2010; Lee et al., 2006; Radice et al., 2013). Deviations from Einstein conjecture were reported by Habersack (2001) in one of the first reports on step lengths and rest periods using tracers in the field.

It is worth discussing the reason why ω has a negative value. Once small particles are dislodged, they are transported for long distances, before coming to rest. This is consistent with what is shown in Figure 10 and with the outcomes of recent works (e.g., Vázquez-Tarrio et al., 2019). The value obtained for c is higher than the average distance between steps in Estero Morales, which is around 10 m. The spacing between pools is a relevant geomorphic dimension of step-pool sequences, given that it is closely related to step formation (Curran, 2007) and flow resistance (Giménez-Curto & Corniero, 2006). During a given ordinary glacier melting induced flood, the tracer displacements are influenced by the bed morphology and selected according to the grain size. Pools are particularly difficult to pass, and it is where coarse particles are more likely found.

Habersack (2001) dealt with Einstein predictors using field data by radio-tracking gravel particles in a large braided river and gather

hundreds of direct measurements of resting times and flight distances. Interestingly, although working in a different bedform setting (i.e., dunes, gravel sheets, and bars), Habersack (2001) also found a negative relationship between the dimensionless step lengths L_i/D_{50} and scaled particle size (D_i/D_{50}). Through flume experiments, Pyrcie and Ashmore (2003) showed that the distribution of mean flight length is related to pool-bar spacing and that only a small proportion of particles are able to move beyond the first bar downstream from the entrainment site. Present and previous results confirm the dependence of grain flights on morphological features, in particular the control that bedforms can exert on coarse particles, preventing long flights, which support the need for a negative value for the proportionality parameter ω in our generalization of the Einstein relation (equation 20).

It is worth stressing that all results presented here derive from field measurements conducted during ordinary daily floods generated by the glacial melt. Larger events (i.e., intense rainfall events in early autumns in the case of the Estero Morales) would result in disruption of the step-pool morphology, deeper sediment active layer, and large erosion/deposition processes in the channel and banks. Under these conditions, the statistical features of sediment displacement lengths and resting times would be likely quite different, and the very premise of the present analysis, that is, the decomposition of the topographic slope, would be affected. It would be interesting to corroborate the Einstein's contention under higher-magnitude events in the Estero Morales when, as in laboratory flume experiments, most of the bed would be mobile.

7. Conclusions

In this work, we presented and analyzed a new data set collected over 2 years of sediment transport monitoring, including PIT-tracer displacements and direct volumetric sampling with Bunte traps, in Estero Morales (Chile). The latter data allowed us to assess the effective slope of the study reach, at least for ordinary floods, and to apply the relation proposed by Meyer-Peter and Müller to successfully predict sediment discharge. This physically based method of breaking down the total (or geometric) slope yielded results that are in good agreement with previous formulations and can be tested straightforwardly in other streams, provided a meter gauge is installed in the reach and volumetric samples of bed load are taken in a range of discharges. We further presented the link between Einstein's predictors and virtual velocity. Frequent tracking of tracer positions, along with the regularity of daily floods in Estero Morales, allowed us to collect a first sample of resting times. Then, by adopting a generalized version of Einstein's fundamental law, we inferred the probabilistic distribution of resting times and flight distances from inter-survey data of tracer displacements. Our results contradict Einstein's assumption and show a surprising decrease in flight distances with larger grain sizes, as opposed to a linear increase. This finding is conceptually consistent with the notion that bed macroroughness, which is responsible for slope decomposition, plays a prominent role in processes that characterize sediment transport, like entrainment and deposition. We also observed that resting times do not depend significantly on tracer size.

Acknowledgments

This work was supported by the project Fondecyt Regular (1170657). We thank Joaquin Lobato, Juan Pablo del Pedregal, Enzo Montenegro, Paolo Bertonecello, and Riccardo Rainato for their help in the field. We are grateful to the Chilean National Park Service (CONAF) for providing access to the sample locations and on-site support of our research. Two anonymous reviewers, John Laronne, and the Associate Editor Luca Solari are thanked for providing several constructive commentaries on a first version of the manuscript. The data from field measurements are available for download in an online open data repository (DOI: 10.5281/zenodo.3274762).

References

- Andrews, E. D. (1983). Entrainment of gravel from naturally sorted riverbed material. *Geological Society of America Bulletin*, 94, 1225–1231.
- Badoux, A., Andres, N., & Turowski, J. M. (2014). Damage costs due to bedload transport processes in Switzerland. *Natural Hazards and Earth System Sciences*, 14, 279–294. <https://doi.org/10.5194/nhess-14-279-2014>
- Batalla, R. J., & Martin-Vide, J. P. (2001). Thresholds of particle entrainment in a poorly sorted sandy gravel-bed river. *Catena*, 44(3), 223–243. [http://doi.org/10.1016/S0341-8162\(00\)00157-0](http://doi.org/10.1016/S0341-8162(00)00157-0)
- Berzi, D., & Fraccarollo, L. (2013). Inclined, collisional sediment transport. *Physics of Fluids*, 25(10), 106601. <http://doi.org/10.1063/1.4823857>
- Bradley, D. N., Tucker, G. E., & Benson, D. A. (2010). Fractional dispersion in a sand bed river. *Journal of Geophysical Research*, 115, F00A09. <https://doi.org/10.1029/2009JF001268>
- Brardinoni, F., & Hassan, M. A. (2007). Glacially induced organization of channel-reach morphology in mountain streams. *Journal of Geophysical Research*, 112, F03013. <https://doi.org/10.1029/2006JF000741>
- Brenna, A., Surian, N., & Mao, L. (2019). Virtual velocity approach for estimating bed material transport in gravel-bed rivers: Key factors and significance. *Water Resources Research*, 55, 1651–1674. <https://doi.org/10.1029/2018WR023556>
- Buffington, J. M., & Montgomery, D. R. (1997). A systematic analysis of eight decades of incipient motion studies, with special reference to gravel-bedded rivers. *Water Resources Research*, 33(8), 1993–2029. <http://doi.org/10.1029/96WR03190>
- Bunte, K., Abt, S. R., Potyondy, J. P., & Ryan, S. E. (2004). Measurement of coarse gravel and cobble transport using portable bedload traps. *Journal of Hydraulic Engineering*, 130(9), 879–893. [http://doi.org/10.1061/\(ASCE\)0733-9429\(2004\)130\(9\)879](http://doi.org/10.1061/(ASCE)0733-9429(2004)130(9)879)
- Campagnol, J., Radice, A., & Ballio, F. (2012). Scale-based statistical analysis of sediment fluxes. *Acta Geophysica*, 60(6), 1744–1777. <http://doi.org/10.2478/s11600-012-0028-6>
- Canovaro, F., Paris, E., & Solari, L. (2007). Effects of macro-scale bed roughness geometry on flow resistance. *Water Resources Research*, 43, W10414. <https://doi.org/10.1029/2006WR005727>
- Capart, H., & Fraccarollo, L. (2011). Transport layer structure in intense bed-load. *Geophysical Research Letters*, 38, L20402. <http://doi.org/10.1029/2011GL049408>
- Chapuis, M., Bright, C. J., Hufnagel, J., & Macvicar, B. (2014). Detection ranges and uncertainty of passive radio frequency identification (RFID) transponders for sediment tracking in gravel rivers and coastal environments. *Earth Surface Processes and Landforms*, 39(15), 2109–2120. <http://doi.org/10.1002/esp.3620>
- Chiari, M., Friedl, K., & Rickenmann, D. (2010). A one-dimensional bedload transport model for steep slopes. *Journal of Hydraulic Research*. <http://doi.org/10.1080/00221681003704087>
- Chiari, M., & Rickenmann, D. (2011). Back-calculation of bedload transport in steep channels with a numerical model. *Earth Surface Processes and Landforms*. <http://doi.org/10.1002/esp.2108>
- Chin, A., & Wohl, E. (2005). Toward a theory for step pools in stream channels. *Progress in Physical Geography*, 29(3), 275–296.
- Church, M. (2006). Bed material transport and the morphology of alluvial river channels. *Annual Review of Earth and Planetary Sciences*, 34(1), 325–354. <http://doi.org/10.1146/annurev.earth.33.092203.122721>
- Church, M., & Hassan, M. A. (1992). Size and distance of travel of unconstrained clasts on a streambed. *Water Resources Research*, 28, 299–303.
- Church, M., & Zimmermann, A. (2007). Form and stability of step-pool channels: Research progress. *Water Resources Research*, 43, W03415. <http://doi.org/10.1029/2006WR005037>
- Comiti, F., Cadol, D., & Wohl, E. (2009). Flow regimes, bed morphology, and flow resistance in self-formed step-pool channels. *Water Resources Research*, 45, W04424. <http://doi.org/10.1029/2008WR007259>
- Comiti, F., & Mao, L. (2012). Recent advances in the dynamics of steep channels. In M. Church, P. M. Biron, & A. G. Roy (Eds.), *Gravel-bed rivers: Processes, tools, environments* (Chap. 26, pp.353–374). Chichester, UK: John Wiley & Sons, Ltd.
- Curran, J. C. (2007). Step-pool formation models and associated step spacing. *Earth Surface Processes and Landforms*, 32(11), 1611–1627. <http://doi.org/10.1002/esp.1589>
- Dell'Agnese, A., Brardinoni, F., Toro, M., Mao, L., Engel, M., & Comiti, F. (2015). Bedload transport in a formerly glaciated mountain catchment constrained by particle tracking. *Earth Surface Dynamics*, 3(4), 527–542. <http://doi.org/10.5194/esurf-3-527-2015>
- Dell'Agnese, A., Mao, L., & Comiti, F. (2014). Calibration of an acoustic pipe sensor through bedload traps in a glacierized basin. *Catena*, 121, 222–231.
- Einstein, H. A. (1950). The bed-load function for sediment transportation in open channel flows. Soil Conservation Service, no. 1026.
- Escauriaza, C., Paola, C., & Voller, V. R. (2017). Computational models of flow, sediment transport and morphodynamics in rivers. In *Gravel-bed rivers: Process and disasters* (pp. 1–31). Hoboken, NJ. <http://doi.org/10.1002/9781118971437.ch1>
- Ferguson, R. (2007). Flow resistance equations for gravel- and boulder-bed streams. *Water Resources Research*, 43, W05427. <http://doi.org/10.1029/2006WR005422>
- Fraccarollo, L., & Hassan, M. A. (2019). Einstein conjecture and resting-time statistics in the bed-load transport of monodispersed particles. *Journal of Fluid Mechanics*, 876, 1077–1089.
- Giménez-Curto, L. A., & Corniero, M. A. (2006). Comment on “characteristic dimensions of the step-pool bed configuration: An experimental study” by Joanna C. Curran and Peter R. Wilcock. *Water Resources Research*, 42, W03601. <http://doi.org/10.1029/2005WR004296>
- Green, K., Alila, Y., & Brardinoni, F. (2015). Patterns of bedload entrainment and transport in forested headwater streams of the Columbia Mountains, Canada. *Earth Surface Processes and Landforms*, 40(4), 427–446.
- Green, K. C., Brardinoni, F., & Alila, Y. (2013). Channel morphology and bed-load yield in fluvial, formerly-glaciated headwater streams of the Columbia Mountains, Canada. *Geomorphology*, 188, 96–109.
- Habersack, H. M. (2001). Radio-tracking gravel particles in a large braided river in New Zealand: A field test of the stochastic theory of bed load transport proposed by Einstein. *Hydrological Processes*, 15(3), 377–391.
- Haschenburger, J. K., & Church, M. (1998). Bed material transport estimated from the virtual velocity of sediment. *Earth Surface Processes and Landforms*, 23(9), 791–808. [http://doi.org/10.1002/\(SICI\)1096-9837\(199809\)23:9<791::AID-ESP888>3.0.CO;2-X](http://doi.org/10.1002/(SICI)1096-9837(199809)23:9<791::AID-ESP888>3.0.CO;2-X)
- Hassan, M. A., Bradley, D. N. (2017). Geomorphic controls on tracer particle dispersion in gravel bed rivers. In *Gravel-bed rivers: Process and disasters* In Tsutsumi, D. & Laronne, J. B. (Eds.), (Chap. 6, pp. 159–184). Hoboken, NJ: Wiley-Blackwell.
- Hassan, M. A., Voepel, H., Schumer, R., Parker, G., & Fraccarollo, L. (2013). Displacement characteristics of coarse fluvial bed sediment. *Journal of Geophysical Research: Earth Surface*, 118, 1–11. <http://doi.org/10.1029/2012JF002374>
- Hohermuth, B., & Weitbrecht, V. (2018). Influence of bed-load transport on flow resistance of step-pool channels. *Water Resources Research*, 54, 5567–5583. <http://doi.org/10.1029/2017WR021523>

- Houbrechts, G., Van Campenhout, J., Levecq, Y., Hallot, E., Peeters, A., & Petit, F. (2012). Comparison of methods for quantifying active layer dynamics and bedload discharge in armoured gravel-bed rivers. *Earth Surface Processes and Landforms*, 37(14), 1501–1517. <http://doi.org/10.1002/esp.3258>
- Kumbhakar, M., Kundu, S., & Ghoshal, K. (2018). An explicit analytical expression for bed-load layer thickness based on maximum entropy principle. *Physics Letters A*, 382(34), 2297–2304.
- Lajeunesse, E., Malverti, L., & Charru, F. (2010). Bed load transport in turbulent flow at the grain scale: Experiments and modeling. *Journal of Geophysical Research*, 115, F04001. <http://doi.org/10.1029/2009JF001628>
- Lamb, M. P., Dietrich, W. E., & Venditti, J. G. (2008). Is the critical Shields stress for incipient sediment motion dependent on channel-bed slope? *Journal of Geophysical Research*, 113, F02008. <http://doi.org/10.1029/2007JF000831>
- Laronne, J. B., Garcia, C., & Reid, I. (2001). Mobility of patch sediment in gravel bed streams: Patch character and its implications for bedload. In M. P. Mosley (Ed.), *Gravel-bed rivers V* (pp. 249–289). Wellington, New Zealand: New Zealand Hydrological Society Inc.
- Lee, H. Y., Lin, Y. T., You, J. Y., & Wang, H. W. (2006). On three-dimensional continuous saltating process of sediment particles near the channel bed. *Journal of Hydraulic Research*. <http://doi.org/10.1080/00221686.2006.9521689>
- Lenzi, M. A., Mao, L., & Comiti, F. (2004). Magnitude-frequency analysis of bed load data in an alpine boulder bed stream. *Water Resources Research*, 40, W07201. <https://doi.org/10.1029/2003WR002961>
- Lenzi, M. A., Mao, L., & Comiti, F. (2006). When does bedload transport begin in steep boulder-bed streams? *Hydrological Processes*, 20, 3517–3533.
- Liébault, F., Bellot, H., Chapuis, M., Klotz, S., & Deschâtres, M. (2012). Bedload tracing in a high-sediment-load mountain stream. *Earth Surface Processes and Landforms*. <http://doi.org/10.1002/esp.2245>
- Liébault, F., & Laronne, J. B. (2008). Evaluation of bedload yield in gravel-bed rivers using scour chains and painted tracers: The case of the Esconavette Torrent (Southern French Preadps). *Geodinamica Acta*, 21(1–2), 23–34. <https://doi.org/10.3166/ga.21.23-34>
- Magirl, C. S., Hildale, R. C., Curran, C. A., Duda, J. J., Straub, T. D., Domanski, M., & Foreman, J. R. (2015). Large-scale dam removal on the Elwha River, Washington, USA: Fluvial sediment load. *Geomorphology*, 246, 669–686. <https://doi.org/10.1016/j.geomorph.2014.12.032>
- Maniatis, G., Hoey, T. B., Hassan, M. A., Sventek, J., Hodge, R., Drysdale, T., & Valyrakis, M. (2017). Calculating the explicit probability of entrainment based on inertial acceleration measurements. *Journal of Hydraulic Engineering*, 143, 04016097.
- Mao, L., & Carrillo, R. (2017). Temporal dynamics of suspended sediment transport in a glacierized Andean basin. *Geomorphology*, 287. <http://doi.org/10.1016/j.geomorph.2016.02.003>
- Mao, L., Carrillo, R., Escauriaza, C., & Iroume, A. (2016). Flume and field-based calibration of surrogate sensors for monitoring bedload transport. *Geomorphology*, 253, 10–21. <http://doi.org/10.1016/j.geomorph.2015.10.002>
- Mao, L., Dell’Agnese, A., & Comiti, F. (2017). Sediment motion and velocity in a glacier-fed stream. *Geomorphology*, 291, 69–79.
- Mao, L., Uyttendaele, G. P., Iroumé, A., & Lenzi, M. A. (2008). Field based analysis of sediment entrainment in two high gradient streams located in Alpine and Andine environments. *Geomorphology*, 93(3–4), 368–383. <http://doi.org/10.1016/j.geomorph.2007.03.008>
- Masteller, C. C., Finnegan, N. J., Turowski, J. M., Yager, E. M., & Rickenmann, D. (2019). History-dependent threshold for motion revealed by continuous bedload transport measurements in a steep mountain stream. *Geophysical Research Letters*, 46, 2583–2591. <https://doi.org/10.1029/2018GL081325>
- Meyer-Peter, E., & Muller, R. (1948). Formulas for bed load transport. Proceedings of 2nd meeting of the International Association for Hydraulic Structures Research, Delft, 39–64.
- Monsalve, A., Yager, E. M., & Schmееckle, M. W. (2017). Effects of bed forms and large protruding grains on near-bed flow hydraulics in low relative submergence conditions. *Journal of Geophysical Research: Earth Surface*, 122, 1845–1866. <http://doi.org/10.1002/2016JF004152>
- Monsalve, A., Yager, E. M., Turowski, J. M., & Rickenmann, D. (2016). A probabilistic formulation of bed load transport to include spatial variability of flow and surface grain size distributions. *Water Resources Research*, 52, 3579–3598. <https://doi.org/10.1002/2015WR017694>
- Nikora, V., Habersack, H., Huber, T., & McEwan, I. (2002). On bed particle diffusion in gravel bed flows under weak bed load transport. *Water Resources Research*, 38(6), 1081. <https://doi.org/10.1029/2001WR000513>
- Nitsche, M., Rickenmann, D., Turowski, J. M., Badoux, A., & Kirchner, J. W. (2011). Evaluation of bedload transport predictions using flow resistance equations to account for macro-roughness in steep mountain streams. *Water Resources Research*, 47, W08513. <https://doi.org/10.1029/2011WR010645>
- Parker, G., Klingeman, P. C., & McLean, D. G. D. (1982). Bedload and size distribution in paved gravel-bed streams. *Journal of the Hydraulics Division. American Society of Civil Engineers*. [http://doi.org/10.1061/\(ASCE\)0733-9429\(1983\)109:5\(793\)](http://doi.org/10.1061/(ASCE)0733-9429(1983)109:5(793))
- Phillips, C. B., Martin, R. L., & Jerolmack, D. J. (2013). Impulse framework for unsteady flows reveals superdiffusive bedload transport. *Geophysical Research Letters*, 40, 1328–1333. <https://doi.org/10.1002/grl.50323>
- Pyrce, R. S., & Ashmore, P. E. (2003). Particle path length distributions in meandering gravel-bed streams: Results from physical models. *Earth Surface Processes and Landforms*, 28(9), 951–966.
- Radice, A., Nikora, V., Campagnol, J., & Ballio, F. (2013). Active interactions between turbulence and bed load: Conceptual picture and experimental evidence. *Water Resources Research*, 49, 90–99. <http://doi.org/10.1029/2012WR012255>
- Recking, A., Piton, G., Vazquez-Tarrio, D., & Parker, G. (2016). Quantifying the morphological print of bedload transport. *Earth Surface Processes and Landforms*, 41(6), 809–822. <http://doi.org/10.1002/esp.3869>
- Rickenmann, D., & Recking, A. (2011). Evaluation of flow resistance in gravel-bed rivers through a large field data set. *Water Resources Research*, 47, W07538. <http://doi.org/10.1029/2010WR009793>
- Saletti, M., Molnar, P., Hassan, M. A., & Burlando, P. (2016). A reduced-complexity model for sediment transport and step-pool morphology. *Earth Surface Dynamics*, 4(3), 549–566. <http://doi.org/10.5194/esurf-4-549-2016>
- Schneider, J. M., Rickenmann, D., Turowski, J. M., Schmid, B., & Kirchner, J. W. (2016). Bed load transport in a very steep mountain stream (Riedbach, Switzerland): Measurement and prediction. *Water Resources Research*, 52, 9522–9541. <https://doi.org/10.1002/2016WR019308>
- Singh, A., Fienberg, K., Jerolmack, D. J., Marr, J., & Foufoula-Georgiou, E. (2009). Experimental evidence for statistical scaling and intermittency in sediment transport rates. *Journal of Geophysical Research*, 114, F01025. <http://doi.org/10.1029/2007JF000963>
- Turowski, J. M., Yager, E. M., Badoux, A., Rickenmann, D., & Molnar, P. (2009). The impact of exceptional events on erosion, bedload transport and channel stability in a step-pool channel. *Earth Surface Processes and Landforms*, 34, 1661–1673.
- Vázquez-Tarrio, D., & Menéndez-Duarte, R. (2015). Assessment of bedload equations using data obtained with tracers in two coarse-bed mountain streams (Narcea River basin, NW Spain). *Geomorphology*, 238, 78–93.

- Vázquez-Tarrio, D., Recking, A., Liébault, F., Tal, M., & Menéndez-Duarte, R. (2019). Particle transport in gravel-bed rivers: Revisiting passive tracer data. *Earth Surface Processes and Landforms*, 44(1), 112–128. <http://doi.org/10.1002/esp.4484>
- Vericat, D., Church, M., & Batalla, R. J. (2006). Bed load bias: Comparison of measurements obtained using two (76 and 152 mm) Helley-Smith samplers in a gravel bed river. *Water Resources Research*, 42, W01402. <http://doi.org/10.1029/2005WR004025>
- Wilcock, P. R. (1993). Critical shear stress of natural sediments. *Journal of Hydraulic Engineering*, 119(4), 491–505. [http://doi.org/10.1061/\(ASCE\)0733-9429\(1993\)119:4\(491\)](http://doi.org/10.1061/(ASCE)0733-9429(1993)119:4(491))
- Wilcox, A. C., Wohl, E. E., Comiti, F., & Mao, L. (2011). Hydraulics, morphology, and energy dissipation in an alpine step-pool channel. *Water Resources Research*, 47, W07514. <http://doi.org/10.1029/2010WR010192>
- Wilson, K. C. (1987). Analysis of bed-load motion at high shear stress. *Journal of Hydraulic Engineering*, 113(1), 97–103. [https://doi.org/10.1061/\(ASCE\)0733-9429\(1987\)113:1\(97\)](https://doi.org/10.1061/(ASCE)0733-9429(1987)113:1(97))
- Wong, M., & Parker, G. (2006). Reanalysis and correction of bed-load relation of Meyer-Peter and Müller using their own database. *Journal of Hydraulic Engineering*. [http://doi.org/10.1061/\(ASCE\)0733-9429\(2006\)132:11\(1159\)](http://doi.org/10.1061/(ASCE)0733-9429(2006)132:11(1159))
- Wong, M., Parker, G., DeVries, P., Brown, T. M., & Burges, S. J. (2007). Experiments on dispersion of tracer stones under lower-regime plane-bed equilibrium bed load transport. *Water Resources Research*, 43, W03440. <http://doi.org/10.1029/2006WR005172>
- Yager, E. M., Turowski, J. M., Rickenman, D., & McArdeall, B. W. (2012). Sediment supply, grain protrusion, and bedload transport in mountain streams. *Geophysical Research Letters*, 39, L10402. <http://doi.org/10.1029/2012GL051654>
- Yager, E. M., Venditti, J. G., Smith, H. J., & Schmeeckle, M. W. (2018). The trouble with shear stress. *Geomorphology*, 323, 41–50. <http://doi.org/10.1016/j.geomorph.2018.09.008>